Calculation of positron annihilation characteristics of six main defects in 6*H*-SiC and the possibility to distinguish them experimentally

F. Linez,* I. Makkonen, and F. Tuomisto
Department of Applied Physics, Aalto University School of Science, PO Box 14100, FI-00076 Aalto, Finland
(Received 11 March 2016; revised manuscript received 3 May 2016; published 6 July 2016)

We have determined positron annihilation characteristics (lifetime and Doppler broadening) in six basic vacancy-type defects of 6*H*-SiC and two nitrogen-vacancy complexes using *ab initio* calculations. The positron characteristics obtained allow us to point out which positron technique in the most adapted to identify a particular defect. They show that the coincidence Doppler broadening technique is the most relevant for observing the silicon vacancy–nitrogen complexes, $V_{Si}N_C$, and carbon vacancy–carbon antisite ones, V_CC_{Si}. For the other studied defects, the calculated positron characteristics are found to be too close for the defects to be easily distinguished using a single positron annihilation technique. Then it is required to use complementary techniques, positron annihilation based or other.

DOI: 10.1103/PhysRevB.94.014103

I. INTRODUCTION

The presence of defects in a crystal lattice can strongly impact material properties such as electrical and thermal conductivity, magnetization, or mechanical resistance. The study of defects in semiconductors is thus an important topic for research and development of new electronic and nanoscopic devices. Among all the semiconductors, silicon carbide is one of the most promising for spintronic and photonic applications due to its wide band gap and the spin coherence properties of some of its lattice defects [1,2]. For instance, recently, the silicon vacancy–nitrogen complex has been identified as a potential qubit for quantum computing [3,4]. It is thus essential to be able to identify the defects experimentally to study their properties as well as to ensure the quality of the crystal growth process. This aim can be reached using techniques such as deep level transient spectroscopy [5], positron annihilation spectroscopy [6,7], photoluminescence [8], and electron paramagnetic resonance [9].

In this paper we focus on positron annihilation spectroscopy. This technique uses the positron's ability to be trapped by vacancy-type defects and to annihilate with the surrounding electrons. The measurement of the positron lifetime before annihilation, or of the Doppler broadening of the annihilation line, gives information about the annihilation environment (open-volume size and nature of the atoms surrounding the vacancy) [10]. Sensitive at a concentration level as low as 10^{15} cm^{-3}, these methods have commonly and successfully been used since the mid-1990s to study defects in semiconductors such as Si, Ge, or GaN [11–15].

The identification of the defects by this technique requires calculating the positron annihilation characteristics in the vacancies and in the bulk material [16]. The interpretation of the results can be relatively easy for a monoatomic material such as Si and Ge or more complicated for multiatomic material and complex crystal structures in which vacancies with various nature and geometry can be created. This problem is shared by the other characterization methods but its impact is smaller since the other techniques measure one defect at a time, whereas with positron annihilation spectroscopy all the defect signatures are mixed into one measurement.

Silicon carbide has more than 200 different polytypes. The most complex of the commonly used polytypes is 6*H*-SiC. A number of distinct vacancies (V) can exist in SiC. The basic ones are V_{Si}, V_C, V_CC_{Si}, V_CV_C, and $V_{Si}V_C$, at which vacancy complexes with impurities or doping atoms can be added. These defects can have different positron annihilation characteristics depending on their position and orientation in the anisotropic crystal structure (basal or axial).

To distinguish and identify all these vacancies, we need to calculate their positron annihilation characteristics: positron lifetime and Doppler broadening of the annihilation spectrum. That requires (i) getting a realistic description of the defect and the atom distribution surrounding it and (ii) calculating the electronic and the positron wave functions as well as the electron-positron correlation potential. Several numerical simulations have already been performed to calculate the positron lifetime [17–23]. The methods and approximations used in these works vary significantly concerning especially the level of self-consistency and how the ionic positions are relaxed. The particular combination of approximations used then significantly affects the predicted results and which defects are seen to trap positrons in calculations. A summary of the similarities and differences of these works and ours are discussed in Appendix A, where we also discuss the possible impact of the **k** point sampling used for the positron on the predicted localization.

It must be noted that most works [17,18,20–22] predicting positron lifetimes in SiC have used the semiempiric enhancement factor [24,25] providing by construction a good agreement with experiment. The first works on this purpose were published by Brauer *et al.* [17,18] They calculated the positron lifetime in 3C and 6*H*-SiC lattices for single and divacancies. They compared two calculation methods: the atomic superposition method (ATSUP) [26] with an approximate electronic charge density [17] and the tight-binding linear muffin-tin orbital (TB-LMTO) method with an electronic charge calculated self-consistently [18]. Their calculations did not take into account the atomic relaxation around the vacancies. The agreement in the positron lifetime obtained with the two numerical methods was between 3

*florence.linez@aalto.fi

and 10 ps. A few years later, Staab *et al.* [19] performed calculations using the ATSUP method and the generalized-gradient approximation (GGA) enhancement factor [27]. The basic atomic relaxations (without the influence of the positron) were taken into account. Staab *et al.* obtained positron lifetimes from 8 to 15 ps longer for vacancies when taking into account the relaxation. However, the positron lifetimes they found were similar to those obtained previously by Brauer and coworkers [18]. More recently, Wiktor *et al.* performed fully self-consistent two-component calculations, taking into account the atomic relaxation caused by the presence of the positron [20]. Their results differed clearly from the previous ones, leading to positron lifetimes 30 ps higher than those of Brauer *et al.* [18] and Staab *et al.* [19] and suggesting that the carbon vacancy could trap positrons. Two recent works using similar calculation schemes disagree qualitatively in this respect with the Wiktor *et al.* results [22,23]. Even thought these new results still need to be reviewed, they have the merit to highlight the strong impact that the positron can have on the defect relaxation when it is localized inside.

Concerning the calculation of the Doppler broadening of the annihilation line, only a few works have been performed. Staab *et al.* took an interest in annihilation only with core electrons, while others such as Barbiellini *et al.* [28–30] simulated both valence and core electrons. Their results were compared to two-dimensional (2D) ACAR or coincidence Doppler spectra but none of them discussed on the annihilation fraction with low (so-called *S* parameter) and high-energy electrons (*W* parameter) to help interpret the simple Doppler broadening spectroscopy.

In this paper we report our calculations of the positron annihilation characteristics (lifetime and Doppler broadening) in the common primary vacancies and in two V_{Si}-N complexes, since N is the most common impurity present in SiC. The impact of the defect configuration (axial or basal) as well as the detector resolution and the energy windows used have also been studied. To validate our calculations, we compared the results to experimental data previously published by various authors.

II. METHOD

A. Calculation method

We model the positron states and annihilation in the bulk and defects of 6*H*-SiC using the VASP code [31], the projector-augmented-wave (PAW) method [32], and an orthorombic supercell with 144 atoms [33]. We used the local-density approximation (LDA) [34] to describe electron-electron exchange and correlation. A plane-wave cutoff energy of 400 eV was found sufficient for reaching convergence. The Brillouin zone was sampled using a $3 \times 2 \times 2$ grid. The optimized a and c/a parameter values were found to be 3.060 Å and 4.9107, consistent with previous values in the literature [20].

We model positrons in these systems using a limit of the two-component density-functional theory for electron-positron systems [35], in which a localized positron does not affect the average positron density, and we take the zero-positron density limits of the LDA electron-positron correlation potential and enhancement factor [35]. Due to certain compensation and feedback effects this scheme gives results that are consistent with more self-consistent modeling [36]. We calculate the positron wave function at the Γ ($\mathbf{k} = 0$) point. We relax the defects taking into account the repulsive forces on ions due to the localized positron [37]. The Doppler spectra are calculated using the so-called state-dependent model [38] and reconstructing the accurate all-electron wave functions within the PAW method [37,39]. This method has been successfully used, for example, for GaN [13], InN [40], and Si [41] as well as various metal oxides [42] for which it allowed to identify defect complexes. Prior to comparison with experiments the theoretical spectra are convoluted with the experimental resolution function. The similarities and differences between our method and those used in past works are described in Appendix A and its Table III.

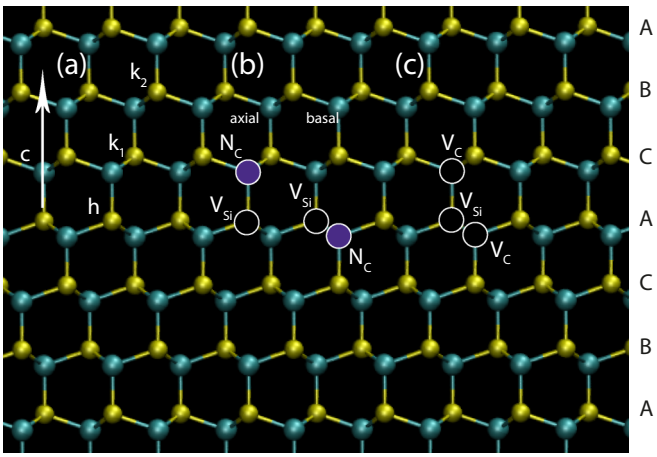

FIG. 1. Stacking sequence in the [1120] plane of 6*H*-SiC illustrating (a) the hexagonal h and quasicubic sites k_1 and k_2, (b) the axial and basal configurations of the V_{Si}-N complex, and (c) the L − shaped trivacancy.

B. Vacancy configurations

The studied defects are the basic V_{Si}, V_C, V_CC_{Si}, V_CV_C, $V_{Si}V_C$, and $V_CV_{Si}V_C$ and two V_{Si}-N complexes. All are neutrally charged. Three different lattice sites exist for each element in the 6*H*-SiC crystal: one hexagonal (h) and two quasicubic sites (k_1 and k_2). In addition, two configurations are also possible for the divacancies and the N complexes: the basal and the axial configuration with the respect to the *c* axis. Figure 1 illustrates the structure and stacking sequence of 6*H*-SiC and how the different defects are aligned in our models. The impact of these different configurations on the positron annihilation characteristics was tested for V_{Si}, $V_{Si}V_C$, and V_{Si}-N.

The positron annihilation characteristics in V_{Si} were calculated for a Si atom removed from hexagonal and quasicubic (k_1) sites [Fig. 1(a)]. The two relaxation steps are detailed in Appendix B. They ended with a slight outward displacement of the C atoms surrounding the vacancy in direction of the bulk [Fig. 2(d)].

The divacancy $V_{Si}V_C$ was modeled in its basal [Fig. 1(b)] and axial [Fig. 1(a)] configurations [Fig. 1(b) shows how the two configurations are aligned relative to the lattice structure]. For the first one, a quasicubic site C vacancy was combined

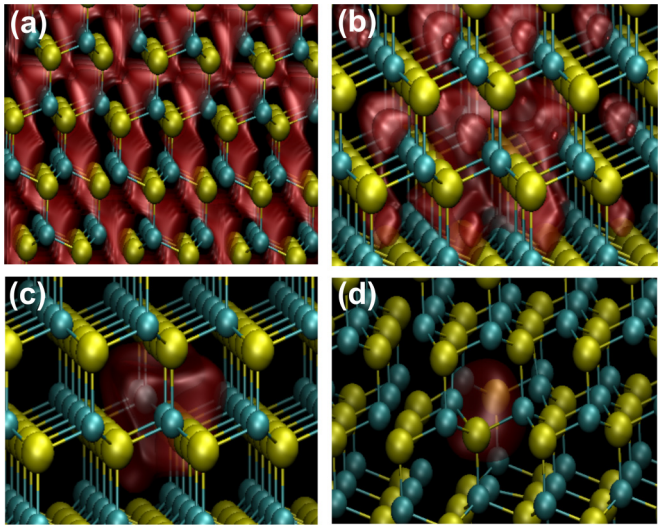

FIG. 2. Positron densities calculated in 576 atoms supercell for (a) the 6*H*-SiC lattice, (b) V_C, (c) V_CV_C, and (d) in a 143-atom cell for V_{Si}^h. Panels (a) and (b) show the delocalized state of the positron in the perfect lattice and as well as in presence of V_C, whereas (c) and (d) show it is trapped in the V_CV_C and the V_{Si}^h.

to a hexagonal Si vacancy. For the second one, both C and Si atoms were removed from a hexagonal site. In both cases, the relaxation leads to a slight enlargement of the free volume left by the missing atoms. The surrounding C atoms moved away from the V_{Si} site (see Appendix B).

The two defect complexes V_{Si}-N are distinguished by the different N atom positions. The first complex, $V_{Si}N^T$, associates a silicon vacancy to a N atom introduced in interstitial position in the closest Si tetrahedral site. During the relaxation processes, the N atom moved toward the Si site nearly in a substitutional position (see Appendix B). Because of that the defect will be next called N_{Si}. In the second vacancy complex, N is introduced in the C substitutional site in the nearest-neighbor shell around the silicon vacancy. This site was reported by Lorenzzi *et al.* as the most stable for the N atom [43]. This defect is noted as $V_{Si}N_C$. This complex was modeled in axial and basal configurations [Fig. 1(b)]. In both cases, the relaxation results in the enlargement of the open volume by the displacement of the N and the C atoms away from the vacancy site.

The four carbon vacancy-based defects V_C, V_CC_{Si}, V_CV_C, and $V_CV_{Si}V_C$ were simulated using only one configuration. The V_C and V_CV_C were modeled removing one and two C atoms from hexagonal sites, respectively. The divacancy was thus in a basal configuration. For both cases, the relaxation leads to a slight reduction of the vacancy volume. V_CC_{Si} corresponds to the transfer of a C atom from a hexagonal site to a close neighbor free hexagonal Si site. The defect has an axial configuration. After the relaxation, the C in the substitutional site has moved to the middle of the three basal surrounding C atoms in an opposite direction from the V_C. As a result, the vacancy has a larger open volume. The trivacancy defect $V_CV_{Si}V_C$ was modeled as an L − shaped vacancy [Fig. 1(c)], superimposing the axial and the basal configurations of $V_{Si}V_C$. The relaxation makes the surrounding carbon atoms go further from the open volume that leads to its slight increase.

TABLE I. Positron lifetime calculated for the bulk and the studied defects. Some results found in the literature are reported for comparison. Most other computational works [17,18,21] use the semiempirical semiconductor correction of the enhancement factor [24,25] resulting in principle in longer positron lifetimes. The same applies to the GGA scheme applied by Staab*et al.* [19]. However, the neglect of relaxation in the early works [17,18] in some cases produces an opposite effect.

Defects	This work (ps)	Theoretical lifetime (ps)	Experimental lifetime (ps)
Lattice	133	131 [19] 141 [17] 144 [21]	136 [44] 140 [6] 146 [45] 144 [46]
V_C	No trapping	153 [17] 183 ± 10 [20] 137 [19]	152 [47] 160 [48]
V_{Si}^h	209	227 [21] 192 [18] 193 [19]	176 [47] 178 [49]
V_{Si}^{k1}	210	183 [17] 195 [19]	183 [44] 210 [48]
$V_{Si}V_C^a$	218	216 [18] 239–241 [21] 213 [19]	209 [49] 225 [6]
$V_{Si}V_C^b$	219	240–241 [21] 216 [19]	
$V_CV_{Si}V_C$	225	250 [21]	
V_CC_{Si}	177		177 [47]
V_CV_C	141		161 [18]
$V_{Si}N_C^b$	209	194 [18]	
$V_{Si}N_C^a$	209	194 [18]	

III. RESULTS AND DISCUSSION

A. Positron lifetime

The first calculation was performed for the defect-free 6*H*-SiC lattice. In this case, the positron lifetime found was 133 ps. This value is in the range 131–144 ps reported in theoretical works using a semiempirical semiconductor correction for the enhancement factor [17,21] but slightly lower than the range 136–146 ps determined in experimental works [6,44–46]. This is also consistent with the tendency of LDA to underestimate the absolute positron lifetime in the lattice.

The positron lifetimes obtained for V_C, V_CV_C, and N_{Si} are close to that of the lattice suggesting that positrons are not trapped by the vacancies and annihilate in a delocalized state. Calculations in a supercell of 576 atoms were performed to verify this point. The positron density obtained in these conditions for the bulk, V_C, and V_CV_C are plotted in Fig. 2 with that of the V_{Si}^h calculated in a 143-atom cell. The results indicate that among V_C, V_CV_C, and N_{Si}, only V_CV_C clearly displays positron trapping. As a result, we do not discuss V_C and N_{Si} positron annihilation characteristics.

Concerning the other defects, the calculated lifetimes are much longer than that of the lattice (see Table I) and the positron annihilates clearly in localized states. The positron lifetime is found to be 218 ps in $V_{Si}V_C$ and 209 ps in V_{Si}.

These values are comparable to those obtained theoretically [18] and experimentally [6,48,49] The comparison between the positron lifetime in V_{Si} and that in $V_{Si}V_C$ shows that adding a carbon vacancy to silicon one changes the lifetime only by 9 ps. The difference is even smaller between $V_{Si}V_C$ and $V_CV_{Si}V_C$. Taking into account the system resolution, the positron source correction, and the lifetime component extraction process, the uncertainty on a positron lifetime measurement from a multicomponent spectrum is about 10 ps, whatever the setup. Consequently, the calculations show that if the two defects are present in a sample, it is not possible to distinguish them by simple positron lifetime measurements.

The positron lifetime calculated in vacancies with various configurations or positions varies only by 1–2 ps. This low impact on the positron lifetime is in agreement with Wiktor *et al.*'s results even if our lifetime values differ [21].

B. Doppler broadening of the annihilation spectrum

The Doppler spectra were calculated in the three orthogonal lattice directions. They were convoluted by a resolution function modeled by a Gaussian curve with a full width at half maximum (FWHM) of 1.25 keV. The Doppler broadening spectra for all the studied vacancies are plotted in Fig. 3. They are presented divided by the Doppler spectrum calculated in the defect-free SiC lattice. The ratio curves associated to V_{Si} and $V_{Si}V_C$ have the two same main peaks centered at 0 and at 1.7 a.u. V_CC_{Si} presents also the same characteristics up to 2.8 a.u., and then the Doppler spectrum is more intense than those of the two others. It should be possible to distinguish V_CC_{Si} from V_{Si} and $V_{Si}V_C$ making coincidence Doppler measurements. Concerning the $V_{Si}N_C$ complexes, the calculations show an impact of the configuration (axial or basal) on the momentum distribution only along directions *a* and *c*. We can also observe that the $V_{Si}N_C$ annihilation spectrum looks like that of V_{Si} but displays a strong dependence of the direction and a higher peak at 1.7 a.u.

The so-called atomic superposition method [26] allows us to estimate the weight of the different shells in the annihilation for momentum higher than about 1.4 a.u. This calculation is less accurate for the low-momentum valence orbitals than the self-consistent calculation. The results plotted in Fig. 4 indicate that the momentum distribution features of the defects is driven by the weight of the positron annihilation with electrons from the shells C 2*s* and C 2*p* compared to those of Si and N shells. In the $V_{Si}N_C$ case, it appears that the difference of peak height observed in Fig. 3 at about 1.7 a.u. is generated by the positron annihilation with electrons from the N 2*p* shell, which competes with those from the C 2*p*. That induces a shift of the W parameter towards higher values, as we will see in Sec. III C. In the case of the divacancy $V_{Si}V_C$ and trivacancy $V_CV_{Si}V_C$, the decreased number of C atoms and their 2*p* shells around the annihilation site contributes together with the increasing open volume to the decrease of the 1.7 a.u. peak height.

The experimental measurement of annihilation spectrum requires performing coincidence measurements by collecting more than 2.5×10^7 counts to reduce the background as much as possible (511 keV-peak/background $> 10^6$) [10]. Indeed, the background affects strongly the wing of the spectrum from about 2.8 a.u., generating the loss of important information.

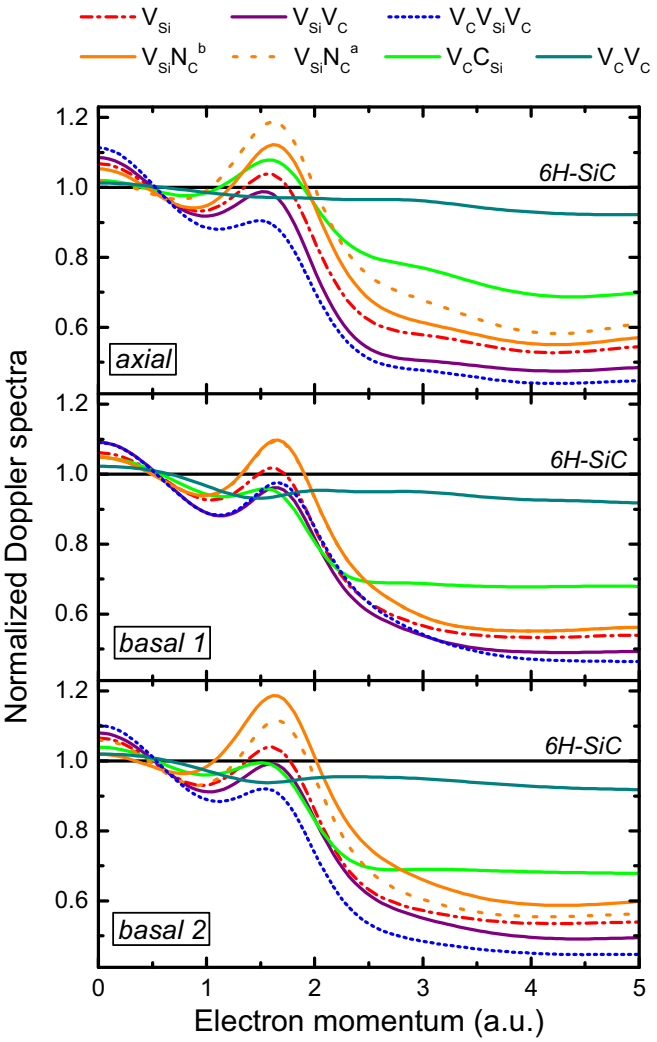

FIG. 3. Ratio curves calculated along the axial (*c* axis) and the two basal directions for all the studied vacancies.

Because these measurements take a lot of time depending on the positron source intensity, one often performs shorter measurements and works with the shape parameters *S* and *W* calculated from the annihilation spectrum. *S* and *W* are defined as the ratio of the number of counts on an energy window to the total number of count in the whole recorded spectrum. The energy windows used in the first part of this work are [510.2;511.8] keV for the *S* parameter and $[504.1; 508.2] \cup [513.8; 517.9]$ keV for the *W* parameter corresponding to $[-0.432; 0.432]$ a.u. and $[-3.726; -1.512] \cup [1.512; 3.726]$ a.u., respectively. We extracted the *S* and *W* parameters from the simulated annihilation spectra in the three directions. Figure 5 shows the average values of the *S* and *W* parameters in the *a* and *b* directions (typical detector position when measuring *c*-axis-oriented single crystal with a slow positron beam) normalized by the average lattice *S* and *W* parameters. As indicated by Fig. 3, the Doppler broadening is anisotropic. This character is not significant for the majority of the studied defects excepted for $V_{Si}N_C$ and $V_CV_{Si}V_C$. For these two defects, the (S,W) points calculated in the *a* and *b* directions are plotted in smaller symbols to illustrate the anisotropy.

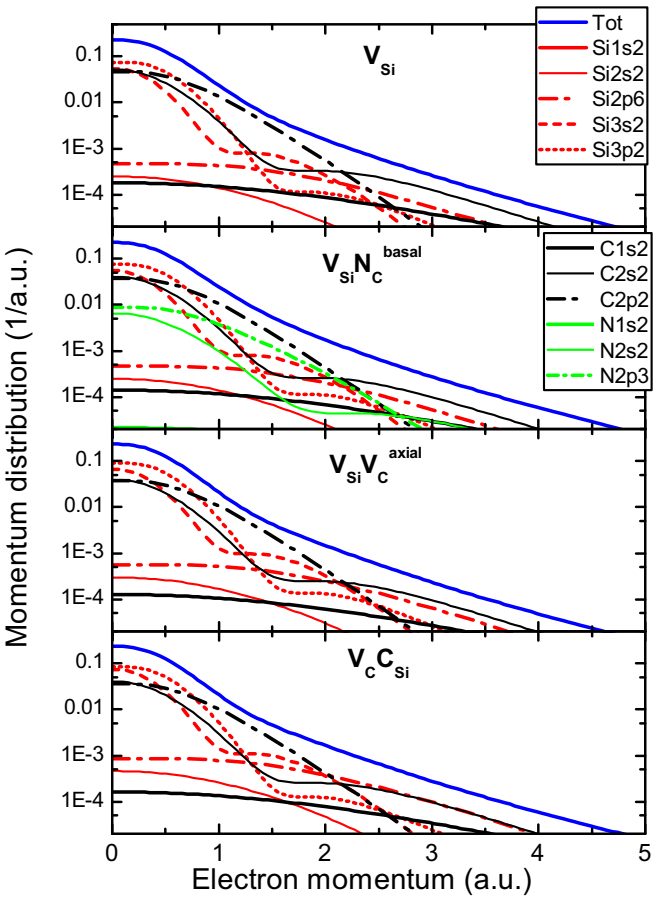

FIG. 4. Weight of the electronic shells involved in the positron annihilation for the studied vacancies.

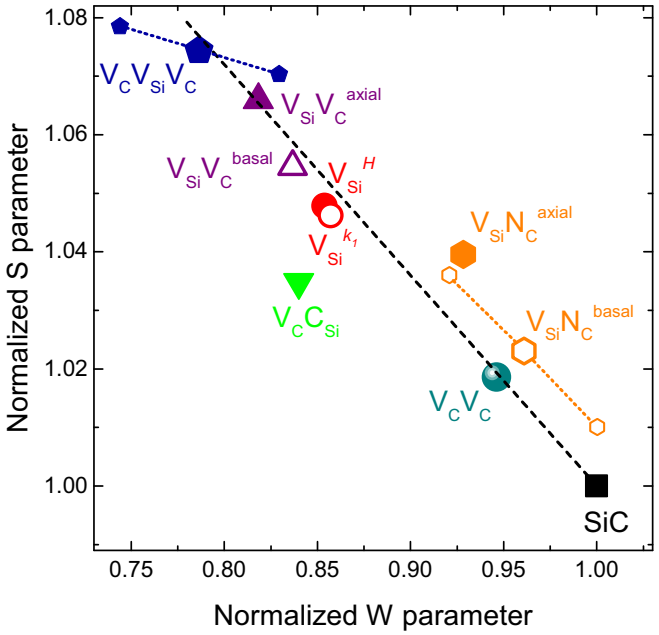

FIG. 5. S and W shape parameters calculated from the simulated spectra for the studied vacancies. The plotted (S,W) pairs correspond to the average value calculated in the a and b crystallographic directions (so-called basal 1 and basal 2 in Fig. 3). The anisotropy being stronger for $V_{Si}N_C$ and $V_CV_{Si}V_C$, the (S,W) values calculated in the a and b directions are also plotted in smaller symbols.

Clearly, we observe that the (S,W) pairs used to identify the defects fall on the SiC-$V_{Si}V_C$ line or in its close vicinity ($\sim$ the measurement dispersion). This implies that it is difficult or even impossible to distinguish the vacancies with only S and W parameters. Indeed, in the case where a fraction of positrons are annihilated in $V_{Si}V_C$, the measured (S,W) values will fall somewhere on the SiC-$V_{Si}V_C$ line. Then, it could be equally well concluded that the positrons annihilate in V_{Si}, $V_{Si}V_C$, or $V_{Si}N_C$. Besides, the results highlight that as for the positron lifetime calculations, increasing the defect size by adding a carbon vacancy to a silicon one does not change strongly the shape parameter values. A modification of the resolution function during a measurement could then prevent the detection of larger vacancies. Finally, the calculations show that the presence of N atoms in a vacancy-complex tends to increase the W parameter.

In conclusion of these two sections (Secs. IIIA and IIIB), our results highlight the difficulty in identifying the nature of the vacancies in 6H-SiC using only one of the positron annihilation techniques. Combining Doppler broadening and positron lifetime can, for defects such as V_CC_{Si} or V_CV_C, allow us to allocate them to V_{Si} or $V_{Si}V_C$. For the detection of N-V complexes, the Doppler broadening in coincidence should be the best of the positron annihilation techniques. Possessing reference samples such as 100% trapping in V_{Si} would be valuable in this aim. In the presence of several kinds of vacancies, the use of complementary techniques, such as electron paramagnetic resonance (EPR) or photoluminescence, or performing positron measurement as a function of the temperature or under illumination (to switch off the signal from some of them [48]) should be envisaged.

C. Impact of the detector resolution and energy windows on the S and W parameters

The Doppler broadening spectrum and the S and W parameters depend strongly on the measurement system resolution and on the energy windows used to define them. The calculations of the shape parameters performed for $V_{Si}V_C^{axial}$, V_{Si}^h, and $V_{Si}N_C^{axial}$ for resolution going from 0.9 and 1.4 keV confirm this tendency. The results presented in Fig. 6 show that the W parameter increases as the resolution function broadens. The changes are significant and V_{Si}^h and $V_{Si}V_C^{axial}$ positron annihilation characteristics could be confused in case the experimental conditions are not taken into account in appropriate manner. A simple theoretical model is examined in Appendix C.

The energy windows used to define the shape parameters are also essential to compare the data obtained with different setups, even in the case of normalized S and W parameters. Figure 7 shows the results of V_{Si}^h S and W parameters for various energy windows. In the Fig. 7(a) only the W energy windows have been changed. The lower bound and the width of the window have a strong impact on the parameter value. This impact depends also on the resolution: the difference between the estimated W values (ΔW) for the studied windows going from 0.16 to 0.23 when the resolution goes from 1.4 to 0.9 keV, respectively. For comparison, the gap between the W parameter of the bulk and that of the divacancy $V_{Si}V_C$ is approximately 0.2. Figure 7(b) shows the changes obtained by enlarging the width of the S energy window from 0.378

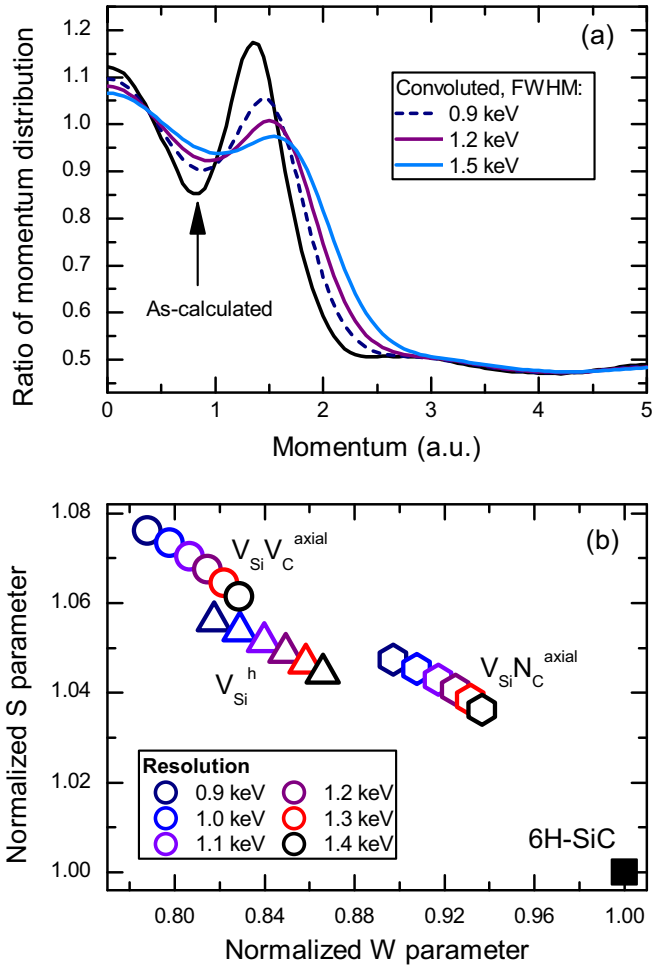

FIG. 6. Impact of the detector resolution on (a) normalized Doppler curves calculated for $V_{Si}V_C^{axial}$ and (b) normalized S and W parameters for $V_{Si}V_C^{axial}$, V_{Si}^h, and $V_{Si}N_C^{axial}$. The results are normalized to a $6H$-SiC calculation convoluted with the same resolution and calculated using the same energy windows.

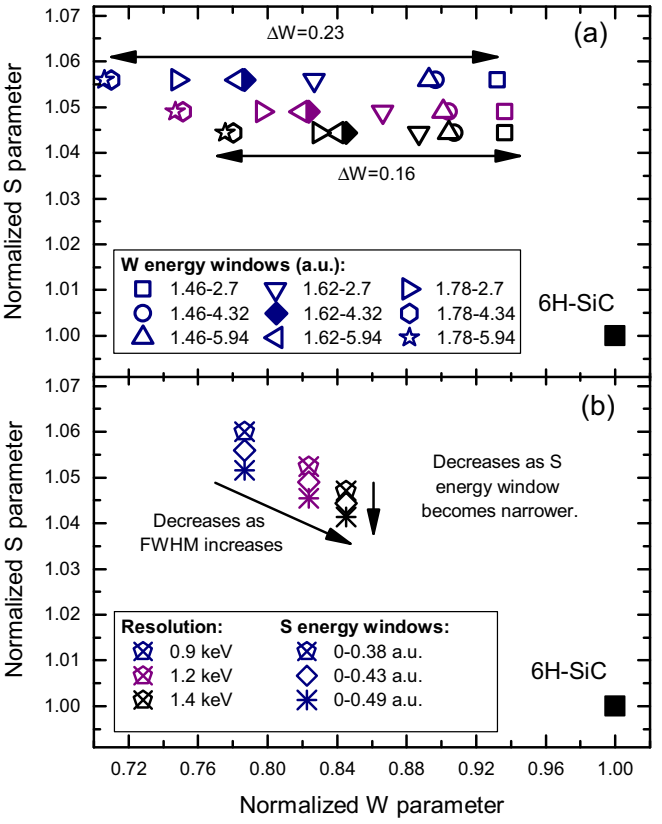

FIG. 7. Normalized S and W parameters calculated from the V_{Si}^h-simulated spectra for various (a) W and (b) S energy windows. The calculation were performed for three resolution values: 0.9, 1.2, and 1.4 keV.

to 0.486 a.u. For these calculations, the W energy windows was fixed at 1.62–4.32 a.u., corresponding to the diamond full symbol in the Fig. 7(a). We notice that the window broadening induces a decrease of the normalized S parameter value ($\Delta S \approx -0.01$) and is slightly more important for the better detector resolution. This shift is in the range of the difference between the S parameters of the V_{Si} and the V_CC_{Si}.

The results of these calculations demonstrate the strong impact of the detector resolution and of the energy windows on the S and W parameters. They highlight that the normalization is not sufficient to get rid of this impact and that comparing Doppler broadening spectroscopy results obtained with different setups requires an accurate knowledge of these two factors. It should be noted that even though the statistical error is not discussed in this work, it should also be taken into account since it impacts strongly the W parameter value and accuracy.

D. Comparison with previous experimental works

First, we compare our calculations with the (S,W) values reported in the literature. Then we compare the relative position of our (S,W) points with studies in which several defects were detected.

To compare quantitatively our results with the (S,W) values found in the literature, we convoluted the simulated annihilation spectra with resolution function reported in the different reports and we determined the S and W parameters with the energy windows defined by the authors. The results of these calculations (S_{calc},W_{calc}) and the experimental values (S_{exp},W_{exp}) are listed in Table II. We note first the large

TABLE II. Comparison with the experimental results found in the literature. We adapt the energy windows and resolutions given by the author.

Suggested defect	S_{exp}	W_{exp}	Ref.	S_{calc}	W_{calc}
V_{Si}(3C)	1.028	0.834	[53]		
V_{Si}(4H)	1.040	0.81	[54]		
V_{Si}(6H)	1.033	0.86	[51]	1.049	0.623
V_{Si}(6H)	1.05	0.9	[47]	1.052	0.801
V_{Si}(4H)	1.060	0.85	[50]	1.043	0.881
$V_{Si}V_C$(6H)	1.068	0.866	[55]	1.070	0.860
$V_{Si}V_C$(4H)	1.070	0.820	[50]	1.059	0.832
V_CC_{Si}(6H)	1.03	1	[47]	1.037	0.790
V_C(6H)	1	1	[47]	1	1

disparity in the experimental values caused by different devices, different energy windows, and different detector resolutions. Then, we observe that the calculated S and W for the divacancy agree very well with the experimental values found by Henry *et al.* [6]. The calculations are also consistent with the Janson *et al.* [50] and Dannefaer and Kerr [47] results, except for the proposed identification of $V_C C_{Si}$, for which the S parameter is correct but the W parameter is lower in our calculations. Nevertheless, our results do not agree at all with those of Kawasuso *et al.* [51]. The calculated W parameter for V_{Si} is dramatically low compared to the experimental values. This could be explained by a low resolution of their spectrometer (between 1.2 and 1.4 keV [52]) or by a mistake in the energy windows' definition or in the defect identification (they might have detected several defects and not only V_{Si}). Except for this last case, our results suggest that, knowing the resolution and the energy windows, we should be able to predict quantitatively the positron annihilation characteristics measured experimentally.

Next we compare the relative position of the positron annihilation characteristics (S, W) for the different defects with experiments where several defects were detected. Janson *et al.* studied the vacancy-type defects induced by ^{11}B, ^{14}N, and ^{27}Al ions implantation in 4H-SiC [50]. They performed Doppler broadening spectroscopy to identify the defects. They observed three main annihilation states associated with the presence of three distinct types of vacancies. These annihilation states are plotted in Fig. 8. The two first were identified as V_{Si} and $V_{Si}V_C$. The third remains unknown but suggests the presence of a larger vacancy than $V_{Si}V_C$ created at a higher fluence than the others. We note that these three (S, W) pairs are all aligned with the bulk annihilation characteristics. This is in complete agreement with our calculations indicating that in silicon carbide all the impurity-free defects fall roughly on a line in the (S, W) plot. The same observation can be extracted from the study of 6H-SiC samples implanted with 50-keV He ions and then annealed at 1400 °C reported in Ref. [7]. After the annealing at high temperature, larger vacancy-type defects were observed with the S and W parameters reaching 1.10 and 0.80, respectively (see Fig. 8). Once again, we note the alignment of the measured positron annihilation characteristics confirming the tendency highlighted by our calculations.

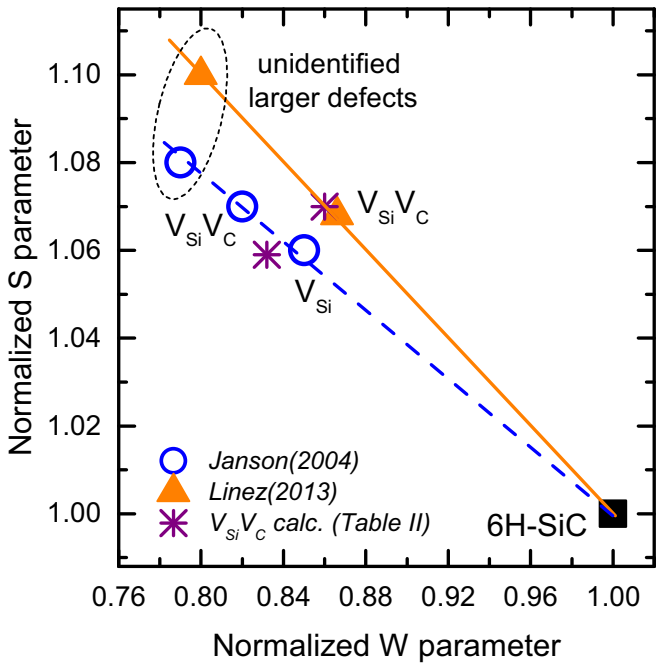

FIG. 8. Comparison of the relative position of positron annihilation characteristics of different vacancies detected by Janson et *al.* [50] and Linez et *al.* [7] in 4H-SiC and 6H-SiC single crystals. The resolutions were 1.3 and 1.24 keV, respectively. The W energy windows differ by 0.2 keV: [513.7;518.0] keV for Linez and [513.8;517.9] keV for Janson. The stars represent the $V_{Si}V_C$ S and W parameters calculated in 6H-SiC for those experimental conditions.

IV. CONCLUSION

In order to identify defects probed by positron annihilation spectroscopy in 6H-SiC, we have calculated the positron annihilation characteristics (Doppler broadening and lifetime) for several basic vacancy-type defects in this material. We have studied the impact of the vacancy configurations as well as that of the detector resolution and of the energy windows defined for the S and W shape parameters.

The positron lifetimes and the broadening shape parameters that we obtained were consistent with the experimental values. By considering different configurations (axial, basal, quasicubic, or hexagonal sites) for V_{Si}, $V_{Si}V_C$, and $V_{Si}N_C$, we found that changing the defect geometry modifies the Doppler broadening parameters only for the vacancy complexes, whereas the positron lifetime is not significantly affected. Our calculations thus bring new reference data and information which will be of use interpreting the positron experiments. For instance, the shift towards the high W parameter value induced by the presence of nitrogen in a carbon site is valuable information to detect and identify the $V_{Si}N_C$ complex and interesting for quantum computing applications.

Nevertheless, our calculations have also highlighted that the lifetimes and the Doppler broadening characteristics of all the studied vacancies, excepted the $V_C V_C$ and the complex $V_C C_{Si}$, are too close to each other to distinguish them accurately. Then, the identification of defects in 6H-SiC proves to be challenging and cannot be deduced from a unique measurement. In addition, we pointed out that the measurements are strongly affected by the detector resolution and the energy windows chosen to define the S and W parameters even when normalized. This can lead to confusing V_{Si}, $V_{Si}V_C$, $V_{Si}N_C$, and even $V_C C_{Si}$.

Using positron annihilation spectroscopy to identify defects in 6H-SiC is challenging. To approach this goal, first, particular attention should be given to the experimental conditions (resolution, energy windows, and direction of measurement). They should be optimized according to which information or vacancy one wants to observe and properly described in all the published works to be able to compare the results. Second, positron annihilation spectroscopy should be adapted using illumination or cooling/heating systems and/or combined with a complementary technique such as photoluminescence or electron paramagnetic resonance.

Work that deals with closely related issues of positron-based identification of defects in SiC was published by Wiktor et *al.* [56] during the review process of this paper.

ACKNOWLEDGMENTS

We acknowledge the computational resources provided by the Aalto Science-IT project and by the Finnish CSC-IT Center for Science. I.M. acknowledges the financial support by the Academy of Finland (Projects No. 285809 and No. 293932).

APPENDIX A: COMPARISON OF THE METHODOLOGIES OF PAST COMPUTATIONAL WORKS

The computational models, approximations and numerical techniques used in past works are summarized in Table III. The level of self-consistency varies in the past calculations between the non-self-consistent ATSUP (Ref. [26]), in which the lattice and potential are composed using a superposition of free atoms; the "conventional scheme" (CONV) used also in this work (for details, see Sec. II A), in which the electronic structure is solved self-consistently but the positron does not affect the average electron density (although its repulsive forces on ions might be taken into account in relaxations, like in this work); and the the fully self-consistent schemes. In the scheme by Puska, Seitsonen, and Nieminen [36] (PSN) one assumes the local-density approximation (LDA) for the electron-positron correlation energy and enhancement factor and uses their two-component parametrizations. The scheme by Gilgien, Galli, Gygi, and Car [57] (GGGC) assumes zero-positron-density limits of functionals and might even self-trap positrons in a defect-free bulk [36]. However, the PSN and CONV schemes have been shown to predict the positron localization in a similar fashion [36], although for systems such as Si and Ge (not as much for SiC) differences have been reported in results and a stronger dependence of the CONV result on the supercell size [22].

Past works have typically used modified or corrected versions of the LDA enhancement factor such as the semiempiric "semiconductor model" [24,25] or the generalized-gradient approximation (GGA) [27], which correct the LDA's underestimation of the positron lifetime.

Concerning the numerical techniques used in the literature, the ATSUP method is based on constructing and solving the positron's Hamiltonian on a real-space grid [26]. Brauer *et al.* [17] used within the CONV scheme the TB-LMTO. The present-day works apply the projector augmented-wave method [32] (PAW). In most implementations, the soft positron state is treated either on a grid (the one used in this work [37] and the one in Ref. [23]) or using plane waves (PW) [22]. Wiktor *et al.* expand also the positron wave function using the PAW method and obtained completeness for both particle types requires special care in creating the PAW construction [58].

One more aspect, whose role in (de-)localizing the positron density in case of small open volume defects, such as carbon vacancy in SiC, should be analyzed in more detail is the significance of the **k** point set used in supercell models for positron states at defects. As discussed before [59], for relatively small supercells the Γ point ($\mathbf{k} = 0$) wave function is too delocalized, whereas a Brillouin zone boundary wave function is too localized (due to the boundary conditions imposed by the periodicity/antiperiodicity of the states). Most computational works do not report at all, which **k** points have been used, whereas some integrate over the whole positron band [58], which in the worst case can give a false indication of trapping (even cause self-trapping in defect-free bulk), if one does not simultaneously monitor the dispersion of the band and perform a convergence test as a function of the cell size using the Γ point only [10].

APPENDIX B: DETAILS OF THE RELAXATION RESULTS

As explained in the text, the lattice relaxation induced by the presence of defect was simulated in two stages. The second stage takes into account the presence of positron which can impact the relaxation by the repulsive Coulumb force on neighboring ions that it generates when it is trapped into a vacancy. The following tables describe more precisely the movement of the atoms surrounding the defect by giving the evolution of the distance between the initial missing atom position and its first and second neighbors. In a perfect lattice, the distance between the Si atom in hexagonal position and its first neighbors is about 1.87 Å and about 3.06 Å for the second-closest neighbors.

TABLE III. A summary of models, approximations and numerical techniques used in the previous computational studies in the literature. The acronyms are defined within the text in Appendix A.

Study	SiC polytypes	Level of e^-–e^+ self-consistency	Numerical method	Ionic relaxations	Enhancement factor
Brauer *et al.* [17]	3C, 6H	CONV	TB-LMTO	Neglected	Semic. model
Brauer *et al.* [18]	3C, 2H, 6*H*	Non-self-consistent	ATSUP	Neglected	Semic. model
Staab *et al.* [19]	4H	Non-self-consistent	ATSUP	e^+ effect Neglected	GGA [27]
Wiktor *et al.* [20,21]	3C, 6*H*	PSN (GGGC tested)	PAW for e^- and e^+	Full	Generalization of the semic. model [20]
Ishibashi and Uedono [22]	3C	PSN	PAW for e^-, PW for e^+	Full	Semic. model
Huang *et al.* [23]	3C	PSN	PAW for e^-, grid for e^+	e^+ effect neglected	Various models compared
Present work	6*H*	CONV	PAW for e^-, grid for e^+	Full	BN-LDA [35]

TABLE IV. Details of the atomic relaxation calculation for the simple defects. The distances are in Å.

	Relax. simple		Relax. with positron	
Defect	First neigh.	Second neigh.	First neigh.	Second neigh.
V_{Si}^{h}	2.04 (+9%)	3.05 (<1%)	2.17 (+16%)	3.08 (<1%)
$V_{Si}^{k_1}$	2.05 (+9%)	3.05 (<1%)	2.18 (+16%)	3.08 (<1%)
V_{C}^{h}	1.87 (<1%)	3.03 (<1%)	1.89 (<1%)	3.04 (<1%)

Table IV gives the magnitude of the relaxation obtained in the case of the single vacancies. In each column, the first value represents the mean distance between the missing atom initial position and the first or second neighbors. The number into brackets indicates the percentage of increase or decrease compared to the initial distance (i.e., perfect in the lattice case).

It appears that the relaxation performed considering the positron enlarges the volume of the vacancy in the V_{Si} case (the nearest-neighbor distances are increased from +9% to +16%), whereas it changes nothing in the V_C. These results are consistent with the fact that the neutrally charged V_C do not trap positrons.

Another piece of information we can extract from the table is that the second-nearest-neighbors circle is not significantly affected by relaxation (distance change <1%).

Table V reports the changes in the interatomic distances for the case of the complex defects. The "Dist." column indicates from which position the distance is calculated: "V_C-*" means that the distance is calculated from V_C (the initial position of the missing atom) to the natural surrounding atoms (in this case, the Si forming the tetrahedron C-Si_4) while "V_C-C_{Si}" corresponds to the particular distance between the missing atom and the antisite.

The results show that only two defects tend to became smaller when relaxing the system: V_CV_C and V_{Si}-N_{Si}^{T}. For the latter, the N atom in the tetrahedral site moves towards the Si vacancy to fill the empty space. Its final location is at 0.38 Å from the substitutional site. The volume of the other defects increases mostly around their V_{Si} part. As for the simple vacancies, taking into account the presence of the positron changes the relaxation in a significant way around a V_{Si} site.

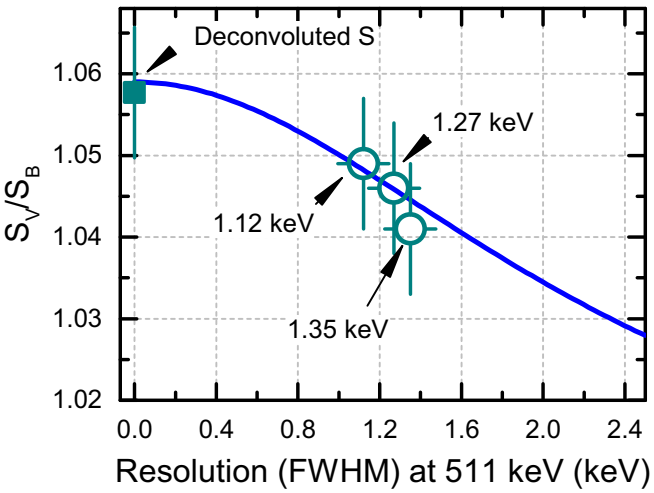

FIG. 9. Evolution of the normalized S parameter as a function of the detector resolution calculated in GaN using the equation (C3) with $\sigma_B^i = 1.0532$ keV ($\sigma \approx$ FWHM/2.35). The open circles are the normalized S parameter measured in the same sample containing V_{Ga} vacancies with three different detectors. The square symbol is the normalized S obtained after deconvolution of the coincidence spectrum [60].

APPENDIX C: SIMPLE THEORETICAL MODEL OF DETECTOR RESOLUTION IMPACT ON THE S PARAMETER.

The resolution of a HPGe detector is typically in the range 1–1.5 keV at 511 keV. The impact of the resolution can be estimated by considering the ideal Doppler spectrum $I(E)$ and the resolution function $R(E)$ are two Gaussian

TABLE V. Details of the atomic relaxation calculation for complex defects. The distances are in Å.

		Relax. simple		Relax. with positron	
Defect	Dist.	First neigh.	Second neigh.	First neigh.	Second neigh.
V_CC_{Si}	V_C-*	–	–	1.98 (+6%)	3.02 (−1%)
	V_C-C_{Si}	–	–	2.57 (+37%)	–
$V_{Si}N_C^a$	V_{Si}-*	2.04 (+9%)	3.04 (<1%)	2.16 (+15%)	3.07 (<1%)
	V_{Si}-N_C	2.11 (+13%)	–	2.20 (+17%)	–
$V_{Si}N_C^b$	V_{Si}-*	2.04 (+9%)	3.04 (<1%)	2.16 (+15%)	3.07 (<1%)
	V_{Si}-N_C	2.11 (+12%)	–	2.19 (+17%)	–
$V_{Si}N_{Si}^T$	V_{Si}-*	1.66 (−11%)	2.99 (−2%)	1.66 (−11%)	2.99 (−2%)
	V_{Si}-N_{Si}^T	0.38 (−80%)	–	0.38 (−80%)	–
V_CV_C	V_C-*	1.84 (−2%)	3.00 (−2%)	1.87 (<1%)	3.01 (−2%)
$V_{Si}V_C^a$	V_{Si}-*	1.99 (+6%)	3.03 (−1%)	2.12 (+13%)	3.06 (<1%)
	V_C-*	1.88 (<1%)	3.03 (<1%)	1.91 (+2%)	3.04 (<1%)
$V_{Si}V_C^b$	V_{Si}-*	2.00 (+7%)	3.03 (<1%)	2.13 (+13%)	3.07 (<1%)
	V_C-*	1.89 (<1%)	3.03 (<1%)	1.92 (+2%)	3.05 (<1%)
$V_CV_{Si}V_C$	V_{Si}	2.05 (+9%)	3.04 (<1%)	1.92 (+2%)	3.00 (−2%)

such as:

$$I(E) = \frac{A}{\sigma^i\sqrt{2\pi}} \exp\left[-\frac{(E-E_0)^2}{2(\sigma^i)^2}\right], \tag{C1}$$

$$R(E) = \frac{B}{\sigma^r\sqrt{2\pi}} \exp\left[-\frac{(E-E_0)^2}{2(\sigma^r)^2}\right], \tag{C2}$$

where E_0 is the peak maximum corresponding to the energy of 511 keV, and $\sigma^{i,r}$ is the standard deviation for the ideal spectrum and resolution function, respectively. The convolution of the two functions gives a third Gaussian with a standard deviation $\sigma^{\text{meas}} = \sqrt{(\sigma^i)^2 + (\sigma^r)^2}$. From Eq. (C2) we can consider that the S parameter is $S \propto 1/\sigma$. Then, the normalization of the S parameter obtained for a vacancy S_V by that measured for the lattice S_B comes down:

$$S_{V/B} = \frac{S_V^{\text{meas}}}{S_B^{\text{meas}}} = \frac{\sigma_B^{\text{meas}}}{\sigma_V^{\text{meas}}} = \sqrt{\frac{\left(\sigma_B^i\right)^2 + (\sigma^r)^2}{\left(\sigma_V^i\right)^2 + (\sigma^r)^2}} = \sqrt{\frac{1 + \left(\sigma^r/\sigma_B^i\right)^2}{\left(1/S_{V/B}^i\right)^2 + \left(\sigma^r/\sigma_B^i\right)^2}}, \tag{C3}$$

where $S_{V/B}^i$ is the normalized S_V in the case of the ideal resolution. Experimentally tested earlier in the case of GaN material, the evolution of $S_{V/B}$ as a function of the detector resolution gives the curve plotted in Fig. 9. The model predicts that the degradation of the detector resolution causes a decrease of the normalized S parameter.

[1] D. Riedel, F. Fuchs, H. Kraus, S. Väth, A. Sperlich, V. Dyakonov, A. A. Soltamova, P. G. Baranov, V. A. Ilyin, and G. V. Astakhov, Phys. Rev. Lett. **109**, 226402 (2012).

[2] W. F. Koehl, B. B. Buckley, F. J. Heremans, G. Calusine, and D. D. Awschalom, Nature **479**, 84 (2011).

[3] F. Fuchs, V. A. Soltamov, S. Väth, P. G. Baranov, E. N. Mokhov, G. V. Astakhov, and V. Dyakonov, Sci. Rep. **3**, 1637 (2013).

[4] L. Gordon, A. Janotti, and C. G. Van de Walle, Phys. Rev. B **92**, 045208 (2015).

[5] G. Alfieri, E. Monakhov, B. Svensson, and M. K. Linnarsson, J. Appl. Phys. **98**, 043518 (2005).

[6] L. Henry, M.-F. Barthe, C. Corbel, P. Desgardin, G. Blondiaux, S. Arpiainen, and L. Liszkay, Phys. Rev. B **67**, 115210 (2003).

[7] F. Linez, E. Gilabert, A. Debelle, P. Desgardin, and M.-F. Barthe, J. Nucl. Mater. **436**, 150 (2013).

[8] S. Castelletto, B. Johnson, V. Ivády, N. Stavrias, T. Umeda, A. Gali, and T. Ohshima, Nat. Mater. **13**, 151 (2014).

[9] H. J. Von Bardeleben, J. L. Cantin, I. Vickridge, and G. Battistig, Phys. Rev. B **62**, 10126 (2000).

[10] F. Tuomisto and I. Makkonen, Rev. Mod. Phys. **85**, 1583 (2013).

[11] M. Fujinami, Phys. Rev. B **53**, 13047 (1996).

[12] S. Eichler, J. Gebauer, F. Börner, A. Polity, R. Krause-Rehberg, E. Wendler, B. Weber, W. Wesch, and H. Börner, Phys. Rev. B **56**, 1393 (1997).

[13] S. Hautakangas, I. Makkonen, V. Ranki, M. J. Puska, K. Saarinen, X. Xu, and D. C. Look, Phys. Rev. B **73**, 193301 (2006).

[14] J. Slotte, M. Rummukainen, F. Tuomisto, V. P. Markevich, A. R. Peaker, C. Jeynes, and R. M. Gwilliam, Phys. Rev. B **78**, 085202 (2008).

[15] K. Saarinen, T. Laine, S. Kuisma, J. Nissilä, P. Hautojärvi, L. Dobrzynski, J. Baranowski, K. Pakula, R. Stepniewski, M. Wojdak *et al.*, Phys. Rev. Lett. **79**, 3030 (1997).

[16] M. Hakala, M. J. Puska, and R. M. Nieminen, Phys. Rev. B **57**, 7621 (1998).

[17] G. Brauer, W. Anwand, E.-M. Nicht, J. Kuriplach, M. Šob, N. Wagner, P. G. Coleman, M. J. Puska, and T. Korhonen, Phys. Rev. B **54**, 2512 (1996).

[18] G. Brauer, W. Anwand, P. G. Coleman, A. P. Knights, F. Plazaola, Y. Pacaud, W. Skorupa, J. Störmer, and P. Willutzki, Phys. Rev. B **54**, 3084 (1996).

[19] T. Staab, L. Torpo, M. Puska, and R. M. Nieminen, in *Materials Science Forum*, Vol. 353 (Trans Tech Publ., 2001), pp. 533–536.

[20] J. Wiktor, G. Jomard, M. Torrent, and M. Bertolus, Phys. Rev. B **87**, 235207 (2013).

[21] J. Wiktor, X. Kerbiriou, G. Jomard, S. Esnouf, M.-F. Barthe, and M. Bertolus, Phys. Rev. B **89**, 155203 (2014).

[22] S. Ishibashi and A. Uedono, in *Journal of Physics: Conference Series*, Vol. 674 (IOP Publishing, Bristol, 2016), p. 012020.

[23] S. Huang, J. Liu, and B. Ye, in *Journal of Physics: Conference Series*, Vol. 674 (IOP Publishing, Bristol, 2016), p. 012022.

[24] M. J. Puska, S. Mäkinen, M. Manninen, and R. M. Nieminen, Phys. Rev. B **39**, 7666 (1989).

[25] M. J. Puska, J. Phys.: Condens. Matter **3**, 3455 (1991).

[26] M. Puska and R. Nieminen, J. Phys. F **13**, 333 (1983).

[27] B. Barbiellini, M. J. Puska, T. Torsti, and R. M. Nieminen, Phys. Rev. B **51**, 7341 (1995).

[28] B. Barbiellini, J. Kuriplach, W. Anwand, and G. Brauer, in *MRS Proceedings*, Vol. 640 (Cambridge University Press, Cambridge, 2000), pp. H5–25.

[29] A. Kawasuso, M. Yoshikawa, H. Itoh, T. Chiba, T. Higuchi, K. Betsuyaku, F. Redmann, and R. Krause-Rehberg, Phys. Rev. B **72**, 045204 (2005).

[30] A. Rubaszek, J. Phys.: Condens. Matter **20**, 335226 (2008).

[31] G. Kresse and J. Furthmüller, Comput. Mater. Sci. **6**, 15 (1996); Phys. Rev. B **54**, 11169 (1996).

[32] P. E. Blöchl, Phys. Rev. B **50**, 17953 (1994); G. Kresse and D. Joubert, *ibid.* **59**, 1758 (1999).

[33] We generated the cell using the CIF2CELL program described in T. Björkman, Comput. Phys. Commun. **182**, 1183 (2011).

[34] J. P. Perdew and A. Zunger, Phys. Rev. B **23**, 5048 (1981).

[35] E. Boroński and R. M. Nieminen, Phys. Rev. B **34**, 3820 (1986).

[36] M. J. Puska, A. P. Seitsonen, and R. M. Nieminen, Phys. Rev. B **52**, 10947 (1995).

[37] I. Makkonen, M. Hakala, and M. J. Puska, Phys. Rev. B **73**, 035103 (2006).

[38] M. Alatalo, B. Barbiellini, M. Hakala, H. Kauppinen, T. Korhonen, M. J. Puska, K. Saarinen, P. Hautojärvi, and R. M. Nieminen, Phys. Rev. B **54**, 2397 (1996).

[39] I. Makkonen, M. Hakala, and M. J. Puska, J. Phys. Chem. Solids **66**, 1128 (2005).

[40] C. Rauch, I. Makkonen, and F. Tuomisto, Phys. Rev. B **84**, 125201 (2011).

[41] M. Rummukainen, I. Makkonen, V. Ranki, M. J. Puska, K. Saarinen, and H.-J. L. Gossmann, Phys. Rev. Lett. **94**, 165501 (2005).
[42] I. Makkonen, E. Korhonen, V. Prozheeva, and F. Tuomisto, J. Phys.: Condens. Matter **28**, 224002 (2016).
[43] J. Lorenzzi, V. Souliere, D. Carole, N. Jegenyes, O. Kim-Hak, F. Cauwet, and G. Ferro, Diam. Relat. Mater. **20**, 808 (2011).
[44] A. Kawasuso, H. Itoh, S. Okada, and H. Okumura, J. Appl. Phys. **80**, 5639 (1996).
[45] A. Rempel and H.-E. Schaefer, Appl. Phys. A **61**, 51 (1995).
[46] S. Dannefaer, W. Puff, and D. Kerr, Phys. Rev. B **55**, 2182 (1997).
[47] S. Dannefaer and D. Kerr, Diam. Relat. Mater. **13**, 157 (2004).
[48] S. Arpiainan, K. Saarinen, P. Hautojärvi, L. Henry, M.-F. Barthe, and C. Corbel, Phys. Rev. B **66**, 075206 (2002).
[49] A. Polity, S. Huth, and M. Lausmann, Phys. Rev. B **59**, 10603 (1999).
[50] M. S. Janson, J. Slotte, A. Y. Kuznetsov, K. Saarinen, and A. Hallén, J. Appl. Phys. **95**, 57 (2004).
[51] A. Kawasuso, F. Redmann, R. Krause-Rehberg, T. Frank, M. Weidner, G. Pensl, P. Sperr, and H. Itoh, J. Appl. Phys. **90**, 3377 (2001).
[52] A. Kawasuso (private communication).
[53] A. Kawasuso, H. Itoh, N. Morishita, M. Yoshikawa, T. Ohshima, I. Nashiyama, S. Okada, H. Okumura, and S. Yoshida, Appl. Phys. A **67**, 209 (1998).
[54] A. Kawasuso, F. Redmann, R. Krause-Rehberg, M. Weidner, T. Frank, G. Pensl, P. Sperr, W. Triftshauser, and H. Itoh, Appl. Phys. Lett. **79**, 3950 (2001).
[55] L. Henry, Structure atomique et activité électrique des défauts natifs et induits par irradiation dans lee carbure de silicium 6H-SiC déterminées par annihilation de positons, Ph.D. thesis, Science and Technology, University of Orléans (2002).
[56] J. Wiktor, G. Jomard, M. Torrent, M.-F. Barthe, and M. Bertolus, Phys. Rev. B **93**, 195207 (2016).
[57] L. Gilgien, G. Galli, F. Gygi, and R. Car, Phys. Rev. Lett. **72**, 3214 (1994).
[58] J. Wiktor, G. Jomard, and M. Torrent, Phys. Rev. B **92**, 125113 (2015).
[59] T. Korhonen, M. J. Puska, and R. M. Nieminen, Phys. Rev. B **54**, 15016 (1996).
[60] J. Kivioja, Master's thesis, Helsinki University of Technology, 2000.